

Single-Particle-Picture Breakdown in laterally weakly confining GaAs Quantum Dots

Daniel Huber,^{1,2,*} Barbara Ursula Lehner,^{1,2} Diana Csontosová,^{3,4} Marcus Reindl,¹ Simon Schuler,¹ Saimon Filipe Covre da Silva,¹ Petr Klenovský,^{3,4,†} and Armando Rastelli^{1,‡}

¹*Institute of Semiconductor and Solid State Physics,
Johannes Kepler University, Linz, Altenbergerstr. 69, 4040, Austria*

²*Secure and Correct Systems Lab, Linz Institute of Technology, Linz, Altenbergerstr. 69, 4040, Austria*

³*Department of Condensed Matter Physics, Faculty of Science,
Masaryk University, Kotlářská 267/2, 61137 Brno, Czech Republic*

⁴*Czech Metrology Institute, Okružní 31, 63800 Brno, Czech Republic*

We present a detailed investigation of different excitonic states weakly confined in single GaAs/AlGaAs quantum dots obtained by the Al droplet-etching method. For our analysis we make use of temperature-, polarization- and magnetic field-dependent μ -photoluminescence measurements, which allow us to identify different excited states of the quantum dot system. Besides that, we present a comprehensive analysis of g-factors and diamagnetic coefficients of charged and neutral excitonic states in Voigt and Faraday configuration. Supported by theoretical calculations by the Configuration interaction method, we show that the widely used single-particle Zeeman Hamiltonian cannot be used to extract reliable values of the g-factors of the constituent particles from excitonic transition measurements.

I. INTRODUCTION

Within the last years GaAs quantum dots (QDs), obtained with the droplet-etching method¹⁻³, emerged as a promising source of non-classical states of light, such as single photons with a strongly suppressed multi-photon emission probability⁴, highly indistinguishable photon states⁵⁻⁸, and single polarization entangled photon-pairs with a near unity degree of entanglement^{5,9-11}.

Only recently it was realized that excitons must be weakly confined in these QDs, as the measured ground-state exciton (X) lifetimes of about 250 ps^{5,9,10} are significantly lower than the minimum lifetime expected for a strongly confining system (440 ps)^{6,12}. The morphology of such GaAs/AlGaAs quantum dots (QDs) features in fact a lateral extension to be much larger than the free exciton Bohr radius in GaAs^{3,5,6}. Therefore, the excitonic states are laterally weakly confined and the Coulomb interaction between the charge carriers is supposed to overwhelm quantum confinement effects. In turn, the weak confinement regime is partly responsible for the excellent optical properties of GaAs QDs, as the short lifetime and large in-plane extension of the wavefunction limit the influence of dephasing and structural anisotropies within the QD¹³.

We note that, a standard model system for the weak confinement regime is represented by GaAs QDs formed at thickness fluctuations in thin GaAs/AlGaAs quantum wells¹⁴, which, however, suffer from a poor control of the lateral confinement. Furthermore, the energy separation between confined states and delocalized states is small. In contrast to that, droplet-etched GaAs QDs avoid these issues and provide an ideal system to study the properties of weakly confined excitons.

Besides possible applications of QDs as single photon and entangled photon-pair sources, the spin states of charges confined in a QD may serve as qubits for quantum technology^{15,16}. Moreover, semiconductor QDs

could provide a link between photonic and spin qubits via photon-to-spin conversion¹⁷. Such complex applications require a detailed knowledge about the response of an excited state in the QD to an external magnetic field, which is described by its g-factor and the diamagnetic coefficient. Furthermore, an individual engineering of the contribution of electrons (e^-) and holes (h^+) within a complex to the overall g-factor is desired¹⁸⁻²⁰. Hence, for engineering the magnetic properties of a QD precise measurements are crucial. Usually, to extract the g factors of e^- and h^+ confined in single QDs from photoluminescence (PL) measurements a single-particle (SP) Zeeman Hamiltonian²¹ is employed^{18,19,22,23} (for details about the method we refer the interested reader to Ref.²⁴). However, it is questionable if one can apply such an approach to weakly confining QDs. The knowledge of the magneto-optical properties of GaAs/AlGaAs QDs obtained by droplet etching is restricted to only a few works²⁵⁻²⁷ and a comprehensive analysis is to the best of our knowledge missing.

In this work we first study various excitonic transitions in GaAs QDs via polarization-resolved and temperature-dependent μ -PL measurements, which allow us to identify several charged states such as the positive (X^+) and negative (X^-) trion as well as some of their excited states. We then present a comprehensive study on the magneto-optical properties of the GaAs/AlGaAs QD system. We apply magnetic fields along the QD growth direction [001] (Faraday configuration) and along the [110] direction (Voigt configuration) and extract the diamagnetic coefficients and g-factors of several excited states in the GaAs QDs. To gain more insight into the physical properties of our QDs under an external magnetic field, we complement our experimental study with calculations using the method of Configuration interaction (CI)²⁸⁻³¹. The theoretical results are in good agreement with the experimental data and confirm that correlation effects among the confined carriers have significant influence on the mag-

netic properties. Finally, we demonstrate by experiment and CI calculations that a SP picture, which turns out to be adequate in the case of strongly confining QDs, leads to poor results in a weakly confining system^{21,24,32}.

II. EXPERIMENTAL RESULTS

A. Polarization-resolved and temperature-dependent μ -PL measurements

We begin by characterizing the optical transitions of our GaAs/AlGaAs QDs. The details on the sample growth are given in Ref.¹⁰. For the excitation we use a 532 nm continuous wave laser, which is focused on the sample through an aspheric lens with 0.65 numerical aperture. The low QD density ($\sim 2 \times 10^7 \text{ cm}^{-2}$) allows us to address the emission of single QDs. In above bandgap excitation, e^- and h^+ are mainly generated in the barrier material of the QD, where the carriers subsequently diffuse, partly get trapped by the QD confinement potential, and relax to the low energy levels. The spectrum of a representative QD is shown in Fig. 1. The spectral po-

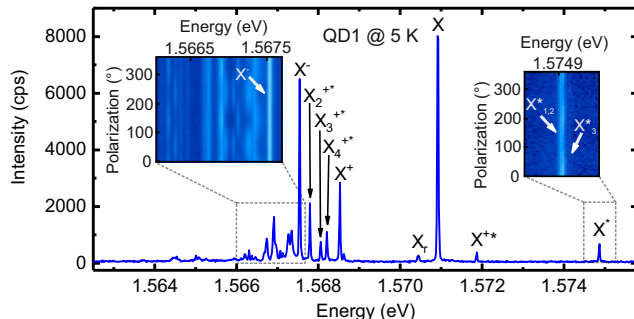


FIG. 1. Spectrum of a representative quantum dot (QD1) under above bandgap excitation at 5 K. The identified recombination channels are labeled within the figure, see text for details. The insets show color-coded μ -PL spectra of transitions within the grey dotted boxes.

sition of X within the cluster of lines is well known from previous experiments^{3,5,6,10}. It has two orthogonally polarized components, which are typically non-degenerate in energy due to the fine structure splitting²¹. The biexciton state is not visible under the used excitation conditions, which we attribute to competition with other configurations due to a slow relaxation of carriers to the ground state via multiple acoustic phonons^{5,6}.

Above-bandgap excitation provides an interesting feature to identify some of the observed transitions: The mobility of e^- and h^+ within the AlGaAs barrier influences the formation probability of the different charge complexes. The mobility is reduced due to scattering events mainly with ionized impurities and phonons, such that the larger scattering cross section of the h^+ com-

pared to the e^- plays a significant role in the spectral response³³. We demonstrate this claim by performing a temperature-dependent μ -PL measurement. By increasing the temperature the mobility of the e^- increases compared to the one for the h^+ and we expect that h^+ -dominated complexes (e. g. X^+) are less often formed than e^- -dominated ones (e. g. X^-).

Fig. 2 shows temperature-dependent μ -PL spectra for temperatures between 5 K and 50 K. The spectra of a

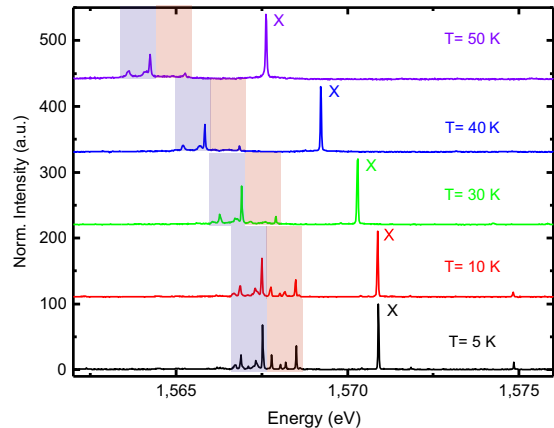


FIG. 2. Normalized temperature-dependent μ -PL spectra of a representative quantum dot (QD1). The quantum dot is excited by a 532 nm continuous wave diode laser above the AlGaAs barrier bandgap.

representative QD (QD1) are normalized with respect to the intensity of the X transition. On the low energy side of the X, transitions with energies $> 1.5675 \text{ eV}$ (see red area in Fig. 2) drop fast in intensity with increasing temperature until they completely disappear. In contrast, transitions with energies $< 1.5675 \text{ eV}$ (see blue area in Fig. 2) are less sensitive to a temperature change.

By combining the temperature-dependence with polarization resolved μ -PL measurements we can now discuss the origin of several transitions in Fig. 1. While the SP picture is poorly suitable for describing the excitonic states of weakly confining QDs⁶, we stick to that for the moment to provide an intuitive description of the charge configuration of the individual states. On the low energy side of X ($< 1.570918 \text{ eV}$ for QD1 at 5 K) we first find a transition labeled as X_r . This feature consists of two linearly-polarized lines with an energy splitting and polarization orientation equal to those of X and disappears under quasi-resonant excitation. We thus attribute it to a quantized energy jitter of the X stemming from charging and uncharging of a defect in the vicinity of the QD. At an energy of 1.568524 eV we then find the X^+ transition and at 1.567542 eV the X^- . We can distinguish between those by the different temperature trend seen in Fig. 2. The trions have no measurable polarization splitting as expected for a Kramers doublet³⁴. Between the trions we observe three additional transitions, which are,

according to the temperature-dependent measurements, h^+ dominated. We thus attribute these lines to the excited states of X^+ (hot trions)^{33–36}. In the SP picture, the simplest hot trion is described by an $e^- - h^+$ pair in the s-shell and an extra h^+ (e^-) in the p-shell. We want to point out that in a more realistic picture including carrier interactions the situation is not that trivial (see Supplementary VI). In most of the QD systems it is difficult to observe radiative transitions from an excited trion as that is converted rapidly to a ground state trion via non-radiative relaxation. However, the slow relaxation rates between the energy levels in our QDs allow us to study these transitions in more detail⁶. Due to exchange interaction, the excited positive trion splits into four degenerated doublets^{34,35}:

$$|X_4^{+*}\rangle = \begin{cases} \uparrow_s (\uparrow_s \downarrow_p - \downarrow_s \uparrow_p) & J_z = +1/2 \\ \downarrow_s (\uparrow_s \downarrow_p - \downarrow_s \uparrow_p) & J_z = -1/2 \end{cases} \quad (1)$$

$$|X_3^{+*}\rangle = \begin{cases} \uparrow_s (\uparrow_s \downarrow_p + \downarrow_s \uparrow_p) & J_z = +1/2 \\ \downarrow_s (\uparrow_s \downarrow_p + \downarrow_s \uparrow_p) & J_z = -1/2 \end{cases} \quad (2)$$

$$|X_2^{+*}\rangle = \begin{cases} \downarrow_s \uparrow_s \uparrow_p & J_z = (+5/2) \\ \uparrow_s \downarrow_s \downarrow_p & J_z = (-5/2) \end{cases} \quad (3)$$

$$|X_1^{+*}\rangle = \begin{cases} \uparrow_s \uparrow_s \uparrow_p & J_z = (+7/2) \\ \downarrow_s \downarrow_s \downarrow_p & J_z = (-7/2) \end{cases} \quad (4)$$

where \uparrow_i, \downarrow_i (\uparrow_i, \downarrow_i) describe the e^- (h^+) spin configuration in the shell $i \in \{s, p\}$ and the number in the brackets gives the total angular momentum projection on the quantization axis under the simplified assumption that holes in the s- and p-states have pure heavy-hole (HH) character (with $J_z = \pm 3/2$). The singlet state (X_4^{+*}) and two of the triplet states (X_3^{+*} and X_2^{+*}) emit a single photon when the s-shell $e^- - h^+$ pair recombines, while the remaining triplet state (X_1^{+*}) is forbidden due to dipole selection rules. Since the energetic ordering of $X_2^{+*} - X_4^{+*}$ is non trivial, we follow the labeling given in Ref.^{35,36}.

Below the X^- we observe several transitions, which, according to the temperature trend, are e^- dominated. Nevertheless, a detailed analysis of these states is not possible in our measurements due to the limited spectral resolution ($\approx 25 \mu\text{eV}$). A polarization resolved μ -PL measurement (see inset Fig. 1) shows non-polarized lines as well as doublets of orthogonally polarized lines. We speculate that these states belong to the excited X^- and/or to multiple negatively charged states.

At energies above the X transition we observe two transitions (X^{+*} and X^*), which disappear with increasing temperature (see Fig. 1). The X^{+*} at 1.571869 eV does not show any polarization splitting. We conclude that this is a transition of an excited X^+ with, where the h^+ in the p-shell recombines with an e^- in the s-shell. The X^*

is a complex of three transitions (see inset Fig. 1), where two ($X_{1,2}^*$ 1.574865 eV) have similar intensities and are orthogonally polarized with an energy splitting of $5 \mu\text{eV}$. The third transition (X_3^* at 1.574931 eV) is linearly polarized and by a factor ~ 15 lower in intensity. This is an excited complex of the bright X doublet (total angular momentum of ± 1) and one component of the dark X doublet (total angular momentum of ± 2), whereby the h^+ of the complex is situated in the p-shell. According to our calculations (discussed later on), we attribute the brightening of one of the nominally dark states to the fact that the p-state holes have 20% light-hole (LH) character, which allows for a weak dipole transition (see Supplementary Section I)²⁵. For clarity, we label the whole transition complex with X^* instead of labeling each transition individually.

B. Magneto-optical properties of GaAs QDs

We continue our study by investigating the magnetic response of the excitonic states discussed above. The QD sample is mounted in a He bath cryostat equipped with a superconducting vector magnet. In Faraday configuration, the magnetic field vector is aligned along the [001] crystal axis (growth direction), which we label as z . Due to the in-plane symmetry of the QDs, we restrict our measurements in Voigt configuration to magnetic fields along [110] crystal axis only, which we label as x . The magnetic field alters the emission properties of the QD, where (i) the diamagnetic shift and (ii) the Zeeman effect are the dominant processes.

In (i) the magnetic field induces a magnetic moment and changes the energy of a state in first approximation according to:

$$\Delta E = \gamma B^2, \quad (5)$$

where γ is the diamagnetic coefficient. For the neutral exciton, the diamagnetic coefficient probes the spatial extent of the excitonic wavefunction, which depends on the spatial confinement and interactions between the confined particles^{37–39}. Hence, it is obvious that the diamagnetic shift is a direction-dependent quantity. The parabolic behaviour from Eq. (5) is only valid in the weak-field limit, where the magnetic length $l_M = \sqrt{\frac{\hbar}{eB}}$ is larger than the spatial extent of the wavefunction l_{wf} ⁴⁰. Note that the magnetic length is $l_M \approx 15 \text{ nm}$ at a magnetic field of 3 T, while the excitonic wavefunction may exceed this value in our GaAs QDs (the QDs have a base diameter of $\approx 60 \text{ nm}$ and a height of $\approx 10 \text{ nm}$), such that the diamagnetic shift can deviate from the B^2 dependence.

In (ii) a magnetic field along z lifts the spin degeneracy, while a field along x also breaks the symmetry of the system introducing a coupling between different states (for example between dark and bright X)^{21,24}. The relation

between magnetic field and splitting (mixing) is characterized by the g-tensor, whereby we probe its elements along x (g_x) and z (g_z)²⁴.

The Zeeman effect in QDs is commonly described by a SP Zeeman Hamiltonian, where the g-factor is a combination of e^- and h^+ g-factors^{21,24}. However, we find in the following that in the weak confinement regime this approximation is not valid.

Fig. 3 shows the shift of the transition lines of QD1 versus the magnetic field between 0 and 2.5 T applied in x - and z -direction, respectively. To get full insight into

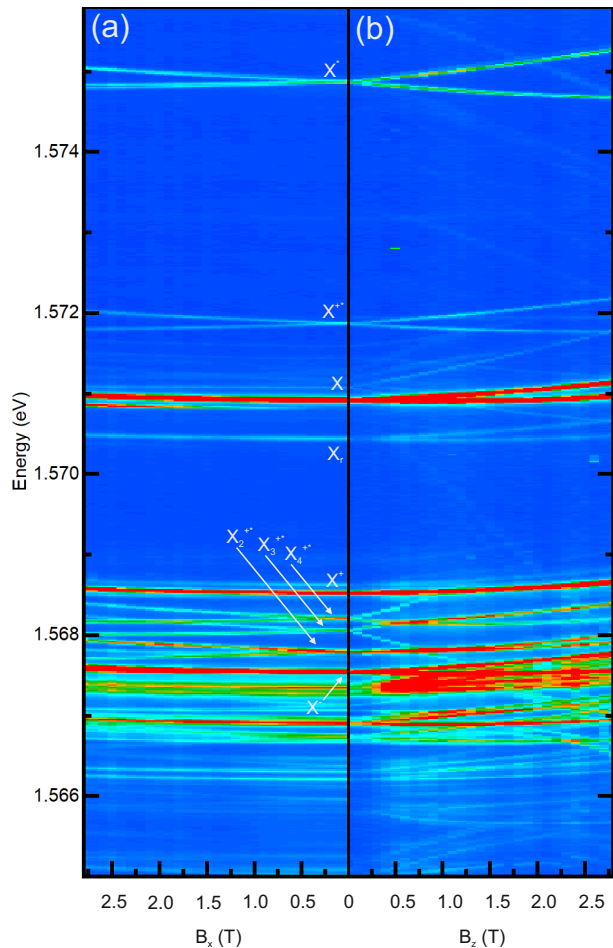


FIG. 3. μ -PL spectra under a magnetic field of a representative QD (QD1) applied along (a) [110] and (b) [001] crystal direction.

the magnetic properties of the different transitions we additionally record polarization-resolved spectra versus magnetic field strength (B). Finally, we use these data to extract the diamagnetic coefficients and g-factors by fitting the energy shifts with the following model⁴¹:

$$E_{\uparrow/\downarrow} = E_0 + \gamma B^2 \pm \frac{1}{2} \sqrt{S^2 + (g_0 + g_2 B^2)^2 \mu_B^2 B^2}, \quad (6)$$

where \uparrow/\downarrow label the two Zeeman-split states, E_0 is the energy of the transition at $B = 0$, g_0 is the g-factor, g_2

is a second order term, S a possible initial fine-structure splitting and μ_B is the Bohr magneton. For convenience, we separate the diamagnetic shift and the Zeeman interaction during fitting by using $\frac{1}{2}(E_{\uparrow} + E_{\downarrow})$ to obtain γ and $E_{\uparrow} - E_{\downarrow}$ to obtain g_0 and g_2 , respectively. In Faraday configuration, the model in Eq. (6) can be used to fit satisfactorily all transitions. However, in Voigt geometry the situation is more complicated due to mixing between the states. We can still use Eq. (6) to fit the X transition for small fields, where the bright-dark mixing is negligible, and also for $X_2^{+*} - X_4^{+*}$, each splitting into two circularly polarized components. The X^+ and X^- , which are not much influenced by the exchange interaction, split instead into four linearly polarized components each, and thus cannot be described by Eq. (6). Therefore we follow the approach outlined in Ref.¹⁹ and calculate the g-factor according to:

$$g_x = \frac{E_1 - E_2}{\mu_B B}, \quad (7)$$

where E_1 (E_2) is the highest (lowest) energy component of the trion quadruplet. We use the same model to extract the g-factors of X^{+*} and X^* , which are found to split into four linearly polarized components. In Tab. I we summarize the results for a representative QD (QD1).

We observe pronounced anisotropies of the g-factors along x and z -direction. This phenomenon has been observed also for other QD systems⁴² and can be *qualitatively* explained in the SP picture following the arguments of Ref.⁴³: the conduction band e^- g-factor is approximately isotropic due to the underlying s-type atomic orbitals; This is not true for the valence band h^+ ^{18,24,44} as the heavy hole (HH) Bloch state has only a projection along the z -direction. Therefore the h^+ g-factor is $g_h \approx 0$ along x , while along z $g_h \gg 0$ is expected⁴⁵. The h^+ ground state in our QDs has a dominant HH character²⁵, so we expect a small value of g_x for X, X^+ , and X^- , which is in line with our measurements. The charged states X^+ and X^- already allow us to observe a discrepancy from the SP picture. Within that simple model the g-factor of the X^+ and X^- is given by $g_{X^+} = g_{e,1} + g_{h,2}$ and $g_{X^-} = g_{e,2} + g_{h,1}$, respectively, whereby $g_{e(h),1}$ is the single e^- (h^+) g-factor in the initial state and $g_{e(h),2}$ the g-factor of the remaining e^- (h^+)⁴⁶. Since the involved e^- and h^+ occupy exclusively the ground s levels, we would expect a similar g-factor for X^+ and X^- , which, however, is not confirmed by our experimental data. Furthermore, X^+ does not even show a significant x - z anisotropy. We want to point out that X^+ , X^- and X are linearly polarized under z -field, which is not expected from SP theory (see Supplementary Section II)²¹. In contrast to that, the transitions X^* , X^{+*} , and $X_2^{+*} - X_4^{+*}$ show a larger g_x . Interestingly, the g-factor anisotropy is reversed for X_2^{+*} . As discussed above, in a SP picture, the $X_2^{+*} - X_4^{+*}$ transitions stem from the recombination of a ground-state electron with a ground-state hole in presence of a hole in the first excited state. The pronounced difference in

TABLE I. The table summarizes fitted diamagnetic coefficients and g-factors for the excitonic transitions in a representative quantum dot (QD1) and the CI calculation results for a magnetic field applied along [110] (x) direction and [001] (z) direction.

QD1	$\gamma_x (\frac{\mu eV}{T^2})$	g_x	$g_{2,x} (T^{-2})$	$\gamma_z (\frac{\mu eV}{T^2})$	g_z	$g_{2,z} (T^{-2})$	CI	$\gamma_x (\frac{\mu eV}{T^2})$	g_x	$g_{2,x} (T^{-2})$	$\gamma_z (\frac{\mu eV}{T^2})$	g_z	$g_{2,z} (T^{-2})$
X*	5.9 (5)	1.61 (3)	-	12.7 (3)	3.74 (1)	-0.01 (1)	X*	4.56	1.7	0.2	14.7	2.57	0.74
X ⁺ *	6.4 (5)	1.45 (3)	-	11.5 (9)	2.58 (1)	-0.01 (1)	X ⁺ *	6.92	0.46	0.03	8.03	0.58	0.12
X	6.4 (1)	0.03 (1)	0.002 (1)	16.81 (7)	1.112 (1)	-0.001 (1)	X	6.46	0.45	0.16	15.6	1.25	0.03
X ⁺	7.6 (7)	0.18 (5)	-	16.29 (4)	0.13 (1)	0.001 (1)	X ⁺	5.8	0.48	0.01	16.17	0.59	0.12
X ₄ ⁺ *	10.4 (3)	1.41 (1)	0.003 (1)	139 (1)	6.33 (1)	0.18 (1)	X ₄ ⁺ *	4.17	1.69	0.04	96.11	2.93	0.87
X ₃ ⁺ *	10.6 (9)	1.13 (5)	0.18 (4)	-94 (1)	8.27 (1)	-0.33 (1)	X ₃ ⁺ *	2.07	1.7	0.07	-55.32	3.31	1.03
X ₂ ⁺ *	6.8 (3)	1.3 (1)	0.01 (1)	20.6 (1)	0.27 (1)	0.04 (1)	X ₂ ⁺ *	7.29	1.66	0.06	10.59	0.64	0.08
X ⁻	6 (1)	0.33 (3)	-	16.9 (5)	1.42 (1)	-0.046 (1)	X ⁻	4.46	0.919	0.0009	15.61	2.12	0.06

the g-factor anisotropy compared to X⁺ clearly indicates that the extra hole is by far not simple "spectator" and that its presence and properties (in particular its significant LH content) has profound effects on the response of the resulting exciton to magnetic fields.

For the higher order excitations of the QD we find that X*, X⁺*, X₄⁺*, and X₃⁺* have larger values of g_z compared to the ground state transitions X, X⁺, X⁻. We attribute this to the LH-HH coupling⁴⁷. In particular, the large g_z value of X₃⁺* leads to a crossing of one of its components with the X⁺ states at moderate magnetic fields. For fields above the crossing point such component disappears, possibly because of efficient relaxation to the lower energy X⁺ state. Furthermore, we observe a coupling between the recombination channels of X* as expected for a complex including a dark state (see Supplementary Section I).

In contrast to our expectations, the diamagnetic shifts are well fitted by Eq. (5) also for high magnetic fields. We find $\gamma_x < \gamma_z$ (except for X₃⁺*). For the neutral X this is qualitatively expected, as the wavefunction is strongly (weakly) confined in z (x) directions, leading to a small (large) γ_x (γ_z). For a charged states, a carrier remains in the QD after e^-h^+ recombination. Hence, the measured γ depends on the localization of the initial as well as the final state. We observe a γ_x which is significantly larger for X₄⁺* and X₃⁺* compared to the other states and an unexpected high γ_z for X₄⁺*. Furthermore, we find a negative diamagnetic coefficient for X₃⁺*. This is known as anomalous diamagnetic shift and was observed for negative trions in InAs/GaAs QDs with weakly confined e^- in the conduction band (see Supplementary Section IV)⁴⁰. In our QDs, we ascribe the anomalous diamagnetic shift to an initial state which is more localized along x than the remaining hole after recombination.

In order to demonstrate that the obtained results are not a feature of a single QD, we extended our study to several QDs (see Supplementary Section III). It turns out that most of the magneto-optical properties are similar, however, we observe significant differences for the excited trion states X₂⁺*-X₄⁺*, indicating a strong dependence on the structural properties of the QD.

As discussed above, the magnetic properties of the trions contradict the SP model. We now demonstrate that the SP Zeeman Hamiltonian is not even sufficient to de-

scribe the magnetic response of a ground state X. We follow Ref.²⁴, where the Hamiltonian of exciton under in-plane magnetic field in the total angular momentum basis is given by:

$$H_B^x = \frac{1}{2} \begin{bmatrix} \delta_0 & \delta_1 & \epsilon_e & \epsilon_h \\ \delta_1 & \delta_0 & \epsilon_h & \epsilon_e \\ \epsilon_e & \epsilon_h & -\delta_0 & \delta_2 \\ \epsilon_h & \epsilon_e & \delta_2 & -\delta_0 \end{bmatrix}, \quad (8)$$

where δ_0 is the splitting between bright and dark exciton states, δ_1 is the exchange splitting between the bright states (fine structure splitting), δ_2 the splitting between the dark states and $\epsilon_{e(h)} = \mu_B B_x g_{e(h),x}$ with $g_{e(h),x}$ the e^- (h^+) g-factor in x -direction. Due to field-induced bright-dark X coupling, in total four dipole transitions are possible. We label the transitions as X_{b i ,2} and X_{d i ,2}, where X_{b i} (X_{d i}) are the transitions of the X complex which are bright (dark) at $B = 0$ and $i = 1, 2$ are the respective orthogonally polarized components. The degree of mixing between bright and dark states depends on B_x and $g_{e,h}$, whereby the intensity of X_{b i ,2} (X_{d i ,2}) is decreasing (increasing) with increasing field. By calculating the eigenvalues of Eq. (8) (see Supplementary Section V) we obtain four equations to fit our measurement data. For the fitting we use the measured values for $\delta_0 = 110 \mu eV$ and $\delta_1 = 4.1 \mu eV$. The value of δ_2 for dark exciton doublet is not known, as in all measured QDs only the X_{d1} component becomes visible, while X_{d2} stays dark (see inset Fig. 4). However, the dark state splitting is supposed to be small and we assume $\delta_2 \approx 0$. Additionally, we find that within a range of 0-20 μeV the influence of δ_2 on the mixing is negligible. We obtain from the fit $|g_{e,x}| = 0.27$ and $|g_{h,x}| = 0.05$. Furthermore, we use the eigenvectors of Eq. (8) to derive the relative oscillator strength (ROS) $\mathcal{R}_{d1,2}$ of X_{d1,2} (see Supplementary Section V), which determines the coupling between dark and bright states. With the measured values for δ_0 and δ_1 given above, $\delta_2 = 0$ and the fitted values of $g_{e,x} = 0.27$ and $g_{h,x} = -0.05$ we obtain the blue and red curve in Fig. 4. Note that we choose the sign of $g_{e,x}$ and $g_{h,x}$ so that the ROS becomes maximal for one component. As expected, the ROS of X_{d1,2} is increasing by ramping up the magnetic field, due to increased mixing between dark and bright X states.

We also calculate from the measurement data the ROS

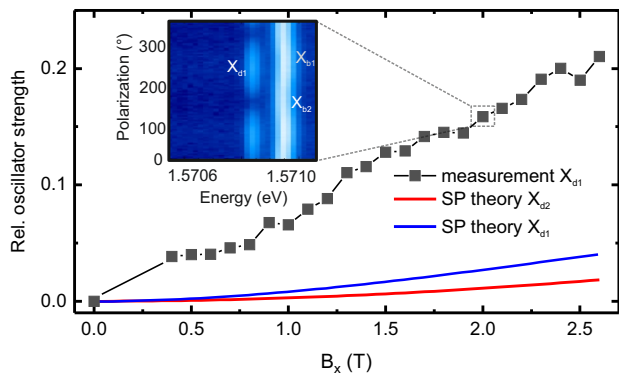


FIG. 4. Relative oscillator strength of the dark exciton state versus magnetic field along [110]. The black squares are the measured values for one dark exciton component (X_{d1}), the second component (X_{d2}) stays dark. The blue (red) curve are the calculated relative oscillator strengths using the e^- and h^+ in-plane g -factors extracted by fitting the measurement data via the SP Zeeman Hamiltonian. The inset shows linear-polarization-resolved spectra $B_x = 2$ T.

according to:

$$\mathcal{R}_{d1} = \frac{I_{X_{d1}}}{I_{X_{d1}} + I_{X_{b1}}}, \quad (9)$$

where $I_{X_{d1,b1}}$ is the intensity of $X_{d1,b1}$. The result is shown in Fig. 4 (black rectangles). Obviously, the measured data do not correspond to the calculated ROS and the coupling between bright and dark states is stronger than expected.

If we use now the ROS equations obtained via the eigenvectors of Eq. (8) (see Supplementary V) and fit the measured trend in Fig. 4 we obtain $g_{h,x} \approx -g_{e,x} \approx 0.52$, which is different from the result obtained by fitting the energy shift with the eigenvalues. Hence, the SP model is not self-consistent and we can conclude that it is not valid in the weak confinement regime. Interestingly, the SP model yields reasonable results for strongly confining GaAs/AlGaAs QDs³².

III. CONFIGURATION INTERACTION CALCULATIONS

To gather a deeper insight in the experimental results and support our claim that the SP model is not suitable to extract single-particle g -factors from PL measurements, we perform calculations combining the 8-band $\mathbf{k}\cdot\mathbf{p}$ method for the computation of single-particle states and the CI method for the excitonic states confined in our weakly confining QDs. On the one hand this approach allows a realistic treatment of the QD shape and composition^{48,49}, including strain and piezoelectricity up to second order^{50–52}. On the other hand it allows an intrinsic treatment of correlation effects, which are included in CI^{31,49} via the excited SP states used to construct the

Slater determinants. This is important, because we expect correlation effects between the confined carriers to play a dominant role in the weak confinement regime.

The simulated QD is composed of pure GaAs embedded in an $\text{Al}_{0.4}\text{Ga}_{0.6}\text{As}$ matrix. Its shape reflects the results of atomic force microscopy measurements on droplet etched nanoholes fabricated under the same growth conditions as the QDs. Additionally, we optimized the structure to match the X emission energy. The final QD shape is such that the QD top is convex while its base is concave (see Supplementary Section VI).

We start out by calculating the SP recombination of X under a magnetic field along z , neglecting Coulomb interaction and correlation. Using Eq. (6) we can extract γ , $g_{2,z}$, and g_z from the computed eigenvalues. The results are presented in Fig. 5. The value of $g_z = 0.6$ (Fig. 5b left panel) as well as $\gamma = 19 \mu\text{eV}/\text{T}^2$ (Fig. 5a left panel) show a significant difference from the measurement data. In the next step we include CI in the simulation, where we start with a SP basis including two e^- and two h^+ (2×2) states and increase it up to twelve e^- and twelve h^+ (12×12) states. In the CI calculation γ (g_z) decreases (increases) by almost one quarter (a factor of two) and approaches a value of $15 \mu\text{eV}/\text{T}^2$ (1.25), which is in good agreement with the measurement. We attribute the decrease of the diamagnetic coefficient to the fact that correlation effects lead to a "shrinkage" of the X wavefunction compared to the bare single particle states, so as to improve the overlap to the hole wavefunction. Furthermore, our calculations point out that the SP model fails to describe the magneto-optical properties in the weak confinement regime and correlation effects cannot be neglected even for the X ground state.

In addition, we use CI to calculate the g -factors and diamagnetic coefficients for the states provided in Tab. I. The results are summarized in the same table (for details on the calculation see Supplementary Section VI), whereby we extend our analysis also to magnetic fields along x . The X^+ g -factor shows only a small x/z anisotropy, which is in good agreement with the experiment. Furthermore, the g -factors of the X^- state are ≈ 2 times larger than the one of the X^+ state, which is not in agreement with the SP description as already discussed in the experimental section.

For the hot trions the CI calculation provides an insight in the origin of large values of γ_z and anomalous diamagnetic shift (see Fig. 5, middle and right panels). These phenomena stem from the mixing of the singlet (X_4^{+*}) and the triplet (X_3^{+*}) trion excited state, an effect that can be traced back to the different magnitude of the electron-hole exchange interaction experienced by each of the two holes constituting hot trion states⁵³. The described effect can happen, e.g., if the excited trion state is spread over a larger region compared to the final hole state. This is the case of the weak confinement which occurs for our QDs in their lateral dimension, hence, the anomalous diamagnetic shift is seen in our case for the Faraday configuration of the applied B field. On the

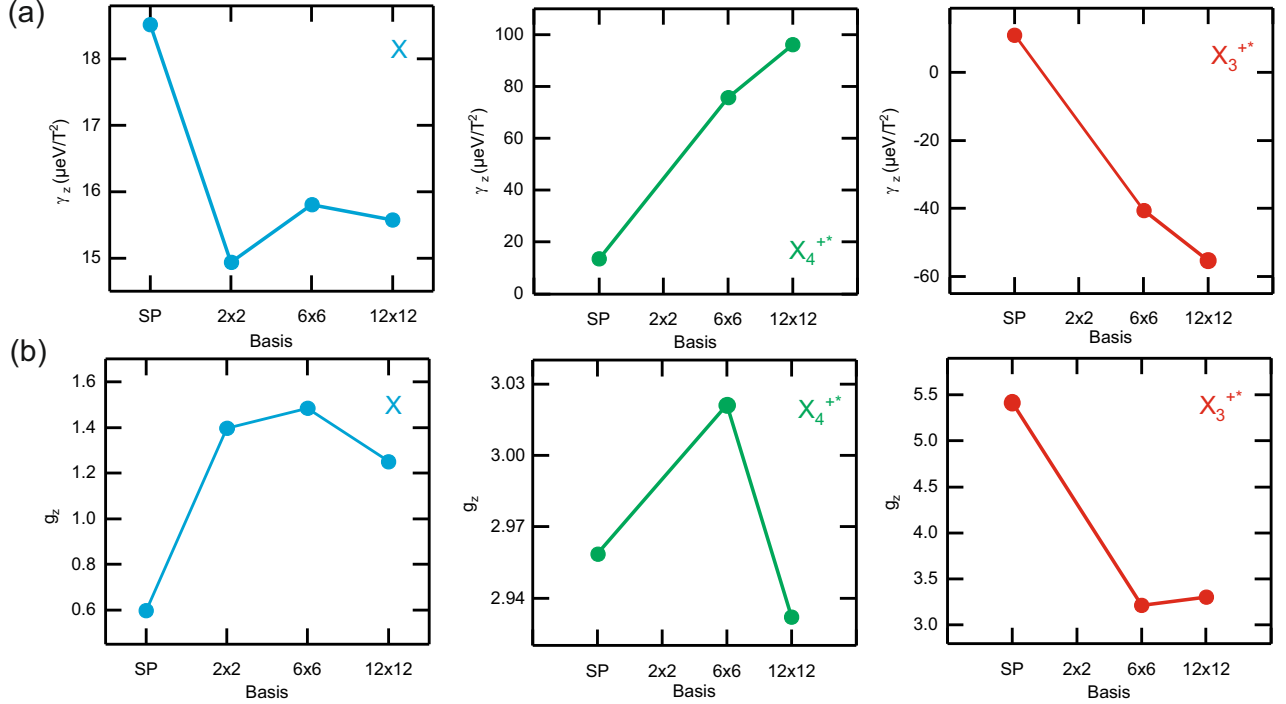


FIG. 5. Magnetic parameters of the groundstate exciton (X) and the excited trion states X_4^{+*} and X_3^{+*} confined in a GaAs QD, calculated with the CI method using single particle states obtained through the $\mathbf{k} \cdot \mathbf{p}$ method for a magnetic field along [001]. The results for γ_z are given in panel (a) and for g_z in (b) for single particle transition (marked by SP on the horizontal axis) and for two electron and two hole (marked by 2x2), six electron and six hole (6x6), and twelve electron and twelve hole (12x12) CI basis. Note that the effect of correlation increases with the basis size, i. e., from SP to (12 x 12) CI basis.

other hand, our QDs are much thinner in the vertical direction and both holes in hot trions are then more strongly confined, with the result that they experience the exchange interaction with electron with equal magnitude. Hence, no large diamagnetic shift is expected for Voigt configuration, exactly as we observe. We stress that the described mixing of singlet and triplet of X^+ for z -direction is a purely multi-particle effect (not describable on SP level) and, moreover, occurs because of the small energy separation between X_4^{+*} and X_3^{+*} as seen in our experiments and calculations, where that amounts to $\approx 100 \mu\text{eV}$ (see Supplementary Section VI). On the other hand the value of g_z is mostly determined by the Zeeman splitting of the final SP hole states that are subtracted from trions (see also Supplementary Section VI).

In general, the simulation results are qualitatively in good agreement with the measurement data. We partly attribute the mismatch in the absolute values between measurement and calculation to differences in the shape and size of the measured and simulated QD. Nevertheless, the CI also shows some deviations from the experiment: Due to the strong confinement along z we would expect similar values for γ_x for all states, which is in line with the measurement. However, we obtain for X_3^{+*} a $\gamma_x = 2 \mu\text{eV}/\text{T}^2$ from the calculations, which is about 3 times smaller than expected. Here the γ_x value directly obtained from the SP states obtained by $\mathbf{k} \cdot \mathbf{p}$ is closer

to the experimental one (see Supplementary Figure 10). Finally we note that, the calculated binding energy of X^+ with respect to the X is only $600 \mu\text{eV}$, whereby all measured QDs show a value of $\approx 2.5 \text{ meV}$. The reason for this deviation is not fully understood yet, but since the problem was observed in independent CI calculations⁵⁴, we speculate that it may stem from an intrinsic limitation of the CI method.

IV. CONCLUSION

In conclusion, we have presented a comprehensive analysis of the optical transitions in a GaAs QD under above bandgap excitation. The performed measurements allow us to determine the charge complexes forming the excited states in a QD. Furthermore, we provide an analysis of the g-factors and diamagnetic coefficients of the excited complexes in our GaAs/AlGaAs QDs obtained by droplet etching. On this basis we are able to experimentally prove that the SP Zeemann Hamiltonian²¹ cannot be used to reliably extract single-particle g-factors from measurements of optical transitions in weakly confining QDs. CI calculations clearly show that interactions between the confined carriers — such as correlation effects — significantly influence the magneto-optical properties. The model calculations are able to quantitatively repro-

duce most of the observed values of diamagnetic shifts and g-factors not only for the neutral excitons, but also for some of the charged complexes observed experimentally. Some significant differences between experiment and calculation results are still present, which deserve further consideration in the future.

ACKNOWLEDGEMENT

We thank L. Vukusic, G. Katsaros, F. Binder and B. Swolo for fruitful discussions and technical assistance.

This work was supported by the austrian science fund (FWF): P29603, the Linz Institute of Technology (LIT)

and the LIT Secure and Correct Systems Lab, financed by the state of Upper Austria.

P.K and D.C received national funding from project CEITEC 2020 (LQ1601) with financial support from the Ministry of Education, Youth and Sports of the Czech Republic under the National Sustainability Programme II and the funding from European Union's Horizon 2020 (2014-2020) research and innovation framework program under grant agreement No 731473. P.K. was (partially) funded by project EMPIR 17FUN06 Siqust. This project has received funding from the EMPIR programme co-financed by the Participating States and from the European Unions Horizon 2020 research and innovation programme.

-
- * daniel.huber@jku.at
 † klenovsky@physics.muni.cz
 ‡ armando.rastelli@jku.at
- ¹ Z. M. Wang, B. L. Liang, K. A. Sablon, and G. J. Salamo, *Applied Physics Letters* **90**, 113120 (2007).
 - ² C. Heyn, A. Stemann, T. Köppen, C. Strelow, T. Kipp, M. Grave, S. Mendach, and W. Hansen, *Applied Physics Letters* **94**, 18 (2009).
 - ³ Y. H. Huo, A. Rastelli, and O. G. Schmidt, *Applied Physics Letters* **102**, 152105 (2013).
 - ⁴ L. Schweickert, K. D. Jns, K. D. Zeuner, S. F. Covre da Silva, H. Huang, T. Lettner, M. Reindl, J. Zichi, R. Trotta, A. Rastelli, and V. Zwiller, *Applied Physics Letters* **112**, 093106 (2018), <https://doi.org/10.1063/1.5020038>.
 - ⁵ D. Huber, M. Reindl, Y. Huo, H. Huang, J. S. Wildmann, O. G. Schmidt, A. Rastelli, and R. Trotta, *Nature Communications* **8**, 15506 (2017).
 - ⁶ M. Reindl, J. H. Weber, D. Huber, C. Schimpf, S. F. Covre da Silva, S. L. Portalupi, R. Trotta, P. Michler, and A. Rastelli, Preprint at: arXiv:1901.11251 (2019).
 - ⁷ E. Schöll, L. Hanschke, L. Schweickert, K. D. Zeuner, M. Reindl, S. F. Covre da Silva, T. Lettner, R. Trotta, J. J. Finley, K. Mller, A. Rastelli, V. Zwiller, and K. D. Jns, *Nano Letters* **19**, 2404 (2019), pMID: 30862165, <https://doi.org/10.1021/acs.nanolett.8b05132>.
 - ⁸ J. Liu, R. Su, Y. Wei, B. Yao, S. Filipe, Y. Yu, J. Iles-smith, K. Srinivasan, A. Rastelli, J. Li, and X. Wang, *Nature Nanotechnology*, 1748 (2019).
 - ⁹ R. Keil, M. Zopf, Y. Chen, B. Höfer, J. Zhang, F. Ding, and O. G. Schmidt, *Nature Communications* **8** (2017).
 - ¹⁰ D. Huber, M. Reindl, S. F. Covre da Silva, C. Schimpf, J. Martín-Sánchez, H. Huang, G. Piredda, J. Edlinger, A. Rastelli, and R. Trotta, *Phys. Rev. Lett.* **121**, 033902 (2018).
 - ¹¹ M. Gurioli, Z. Wang, A. Rastelli, T. Kuroda, and S. Sanguinetti, *Nature Materials* **18**, 799810 (2019).
 - ¹² S. Stobbe, T. W. Schlereth, S. Höfling, A. Forchel, J. M. Hvam, and P. Lodahl, *Phys. Rev. B* **82**, 233302 (2010).
 - ¹³ D. Huber, M. Reindl, J. Aberl, A. Rastelli, and R. Trotta, *Journal of Optics* **20**, 073002 (2018).
 - ¹⁴ E. Peter, P. Senellart, D. Martrou, A. Lemaître, J. Hours, J. M. Gérard, and J. Bloch, *Phys. Rev. Lett.* **95**, 067401 (2005).
 - ¹⁵ D. Loss and D. P. DiVincenzo, *Phys. Rev. A* **57**, 120 (1998).
 - ¹⁶ I. Schwartz, E. R. Schmidgall, L. Gantz, D. Cogan, E. Bordo, Y. Don, M. Zielinski, and D. Gershoni, *Phys. Rev. X* **5**, 011009 (2015).
 - ¹⁷ L. Gaudreau, A. Bogan, M. Korkusinski, S. Studenikin, D. G. Austing, and A. S. Sachrajda, *Semiconductor Science and Technology* **32**, 093001 (2017).
 - ¹⁸ H. M. G. A. Tholen, J. S. Wildmann, A. Rastelli, R. Trotta, C. E. Pryor, E. Zallo, O. G. Schmidt, P. M. Koenraad, and A. Y. Silov, *Phys. Rev. B* **99**, 195305 (2019).
 - ¹⁹ A. J. Bennett, M. A. Pooley, Y. Cao, N. Skld, I. Farrer, D. A. Ritchie, and A. J. Shields, *Nature Comm.* **4**, 1522 (2013).
 - ²⁰ G. Medeiros-Ribeiro, E. Ribeiro, and H. Westfahl Jr., *Applied Physics A* **77**, 725 (2003).
 - ²¹ M. Bayer, G. Ortner, O. Stern, A. Kuther, A. A. Gorbunov, A. Forchel, P. Hawrylak, S. Fafard, K. Hinzer, T. L. Reinecke, S. N. Walck, J. P. Reithmaier, F. Klopff, and F. Schäfer, *Phys. Rev. B* **65**, 195315 (2002).
 - ²² H. M. G. A. Tholen, J. S. Wildmann, A. Rastelli, R. Trotta, C. E. Pryor, E. Zallo, O. G. Schmidt, P. M. Koenraad, and A. Y. Silov, *Phys. Rev. B* **94**, 245301 (2016).
 - ²³ W. Sheng, *Applied Physics Letters* **96**, 133102 (2010), <https://doi.org/10.1063/1.3367707>.
 - ²⁴ B. J. Witek, R. W. Heeres, U. Perinetti, E. P. A. M. Bakkers, L. P. Kouwenhoven, and V. Zwiller, *Phys. Rev. B* **84**, 195305 (2011).
 - ²⁵ Y. H. Huo, B. J. Witek, S. Kumar, J. R. Cardenas, J. X. Zhang, N. Akopian, R. Singh, E. Zallo, R. Grifone, D. Kriegner, R. Trotta, F. Ding, J. Stangl, V. Zwiller, G. Bester, A. Rastelli, and O. G. Schmidt, *Nature Physics* **10**, 4651 (2014).
 - ²⁶ A. Ulhaq, Q. Duan, E. Zallo, F. Ding, O. G. Schmidt, A. I. Tartakovskii, M. S. Skolnick, and E. A. Chekhovich, *Phys. Rev. B* **93**, 165306 (2016).
 - ²⁷ M. C. Löbl, L. Zhai, J.-P. Jahn, J. Ritzmann, Y. Huo, A. D. Wieck, O. G. Schmidt, A. Ludwig, A. Rastelli, and R. J. Warburton, Preprint at: arXiv:1902.10145 (2019).
 - ²⁸ T. Takagahara, *Physical Review B* **47**, 4569 (1993).
 - ²⁹ J. Shumway, A. Franceschetti, and A. Zunger, *Phys. Rev. B* **63**, 155316 (2001).
 - ³⁰ A. Schliwa, M. Winkelnkemper, and D. Bimberg, *Phys.*

- Rev. B **79**, 075443 (2009).
- ³¹ P. Klenovský, P. Steindl, and D. Geffroy, Scientific Reports **7**, 45568 (2017).
- ³² S. Kunz, Magneto-optical properties of individual GaAs/AlGaAs Quantum Dots grown by Droplet Epitaxy, Institut national des sciences appliques de Toulouse (2013).
- ³³ N. I. Cade, H. Gotoh, H. Kamada, H. Nakano, and H. Okamoto, Phys. Rev. B **73**, 115322 (2006).
- ³⁴ K. V. Kavokin, physica status solidi (a) **195**, 592 (2003).
- ³⁵ Y. Igarashi, M. Shirane, Y. Ota, M. Nomura, N. Kumagai, S. Ohkouchi, A. Kirihara, S. Ishida, S. Iwamoto, S. Yorozu, and Y. Arakawa, Phys. Rev. B **81**, 245304 (2010).
- ³⁶ T. Warming, E. Siebert, A. Schliwa, E. Stock, R. Zimmermann, and D. Bimberg, Phys. Rev. B **79**, 125316 (2009).
- ³⁷ M. Bayer, S. N. Walck, T. L. Reinecke, and A. Forchel, Phys. Rev. B **57**, 6584 (1998).
- ³⁸ C. Schulhauser, D. Haft, R. J. Warburton, K. Karrai, A. O. Govorov, A. V. Kalameitsev, A. Chaplik, W. Schoenfeld, J. M. Garcia, and P. M. Petroff, Phys. Rev. B **66**, 193303 (2002).
- ³⁹ M.-F. Tsai, H. Lin, C.-H. Lin, S.-D. Lin, S.-Y. Wang, M.-C. Lo, S.-J. Cheng, M.-C. Lee, and W.-H. Chang, Phys. Rev. Lett. **101**, 267402 (2008).
- ⁴⁰ Y. J. Fu, S. D. Lin, M. F. Tsai, H. Lin, C. H. Lin, H. Y. Chou, S. J. Cheng, and W. H. Chang, Phys. Rev. B **81**, 113307 (2010).
- ⁴¹ J. van Bree, A. Y. Silov, P. M. Koenraad, M. E. Flatté, and C. E. Pryor, Phys. Rev. B **85**, 165323 (2012).
- ⁴² J. van Bree, A. Y. Silov, M. L. van Maasakkers, C. E. Pryor, M. E. Flatté, and P. M. Koenraad, Phys. Rev. B **93**, 035311 (2016).
- ⁴³ A. Schwan, B.-M. Meiners, A. Greilich, D. R. Yakovlev, M. Bayer, A. D. B. Maia, A. A. Quivy, and A. B. Henriques, Applied Physics Letters **99**, 221914 (2011).
- ⁴⁴ C. E. Pryor and M. E. Flatté, Phys. Rev. Lett. **96**, 026804 (2006).
- ⁴⁵ H. Watzinger, C. Kloeffel, L. Vukusic, M. D. Rossell, V. Sessi, J. Kukucka, R. Kirchschrager, E. Lausecker, A. Truhlar, M. Glaser, A. Rastelli, A. Fuhrer, D. Loss, and G. Katsaros, Nano letters **16**, 6879 (2016).
- ⁴⁶ I. A. Akimov, K. V. Kavokin, A. Hundt, and F. Henneberger, Phys. Rev. B **71**, 075326 (2005).
- ⁴⁷ M. Durnev, M. Glazov, and E. Ivchenko, Physica E: Low-dimensional Systems and Nanostructures **44**, 797 (2012).
- ⁴⁸ S. Birner, T. Zibold, T. Andlauer, T. Kubis, M. Sabathil, A. Trellakis, and P. Vogl, IEEE Trans. El. Dev. **54**, 2137 (2007).
- ⁴⁹ Petr Klenovský, Andrei Schliwa, Dieter Bimberg, Phys. Rev. B *in print*, arXiv:1903.09078.
- ⁵⁰ A. Beya-Wakata, P. Y. Prodhomme, and G. Bester, Physical Review B **84**, 195207 (2011).
- ⁵¹ P. Klenovský, P. Steindl, J. Aberl, E. Zallo, R. Trotta, A. Rastelli, and T. Fromherz, Physical Review B **97**, 245314 (2018).
- ⁵² J. Aberl, P. Klenovský, J. S. Wildmann, J. Martín-Sánchez, T. Fromherz, E. Zallo, J. Humlíček, A. Rastelli, and R. Trotta, Phys. Rev. B **70**, 201308 (2017).
- ⁵³ M. Z. Maialle and M. H. Degani, Phys. Rev. B **76**, 115302 (2007).
- ⁵⁴ L. Wang, V. Krápek, F. Ding, F. Horton, A. Schliwa, D. Bimberg, A. Rastelli, and O. G. Schmidt, Phys. Rev. B **80**, 085309 (2009).